JACS
JOURNAL OF THE AMERICAN CHEMICAL SOCIETY

Article

pubs.acs.org/JACS

Superexchange Contributions to Distance Dependence of Electron Transfer/Transport: Exchange and Electronic Coupling in Oligo(*para*-Phenylene)- and Oligo(2,5-Thiophene)-Bridged Donor–Bridge–Acceptor Biradical Complexes

Martin L. Kirk,*[,‡] David A. Shultz,*[,†] Daniel E. Stasiw,[†] Geoffrey F. Lewis,[†,§] Guangbin Wang,[†,∥] Candice L. Brannen,[†,#] Roger D. Sommer,[†] and Paul D. Boyle[†,⊥]

[†]Department of Chemistry, North Carolina State University, 2200 Hillsborough, Raleigh, North Carolina 27695-8204, United States

[‡]Department of Chemistry and Chemical Biology, The University of New Mexico, MSC03 2060, 1 University of New Mexico, Albuquerque, New Mexico 87131-0001, United States

Supporting Information

ABSTRACT: The preparation and characterization of three new donor–bridge–acceptor biradical complexes are described. Using variable-temperature magnetic susceptibility, EPR hyperfine coupling constants, and the results of X-ray crystal structures, we evaluate both exchange and electronic couplings as a function of bridge length for two quintessential molecular bridges: oligo(*para*-phenylene), β = 0.39 Å^{-1} and oligo(2,5-thiophene), β = 0.22 Å^{-1}. This report represents the first direct comparison of exchange/electronic couplings and distance attenuation parameters (β) for these bridges. The work provides a direct measurement of superexchange contributions to β, with no contribution from incoherent hopping. The different β values determined for oligo(*para*-phenylene) and oligo(2,5-thiophene) are due primarily to the D–B energy gap, $\mathbf{\Delta}$, rather than bridge–bridge electronic couplings, $\mathbf{H_{BB}}$. This is supported by the fact that the $\mathbf{H_{BB}}$ values extracted from the experimental data for oligo(*para*-phenylene) ($\mathbf{H_{BB}}$ = 11 400 cm^{-1}) and oligo(2,5-thiophene) (12 300 cm^{-1}) differ by <10%. The results presented here offer unique insight into the intrinsic molecular factors that govern $\mathbf{H_{DA}}$ and β, which are important for understanding the electronic origin of electron transfer and electron transport mediated by molecular bridges.

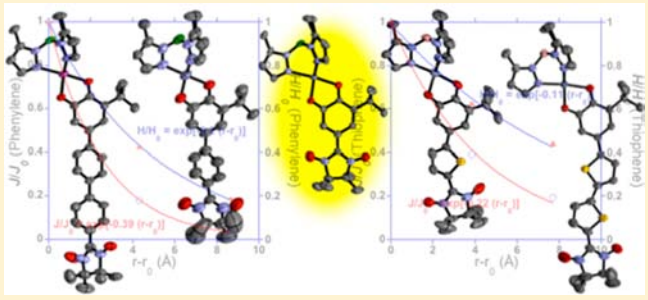

INTRODUCTION

Donor–bridge–acceptor (D–B–A) triads have been used as model systems to evaluate design principles for molecular electronics and photoinduced electron-transfer (PET) reactions.[1−14] However, when both the donor and acceptor are paramagnetic, D–B–A molecules may serve as functional equivalents of charge-separated excited states generated by PET reactions as well as analogs of (spin-polarized) biased, single-molecule electronic devices, Figure 1.[14] Hush has stated that solution electron-exchange processes that occur between aromatic radicals are close to the adiabatic limit except when electron transfer occurs over long distances.[15] As such, it is important to understand the distance dependence of the electronic coupling matrix element, $\mathbf{H_{DA}}$, which is central to our ability to correlate electronic and geometric structure with electron-transfer/-transport properties. Complications arise in the development of these electronic-geometric structure relationships since there are a number of different pathways for bridge-mediated magnetic exchange and molecular electron-transfer/-transport, and each may have their own dependence on orientation and distance.[16] Therefore, it is essential that well-designed molecular systems with known structures be employed in order to quantitatively determine molecular bridge contributions to electronic communication.

Our efforts[14] have combined magnetometry, spectroscopy, theory, and computations to correlate bridge-mediated magnetic exchange and electronic coupling between an S = 1/2 semiquinone (SQ) donor and S = 1/2 nitronylnitroxide (NN) acceptor within the framework of the valence bond configuration interaction (VBCI)[17,18] model. By taking advantage of a single dominant superexchange pathway in our D–B–A biradical systems (e.g., there are up to 25 superexchange pathways in bridged transition-metal dimers), a straightforward relationship can be derived between the electronic coupling matrix element, $\mathbf{H_{DA}}$, and the magnetic exchange coupling, $\mathbf{J_{DA}}$ ($\equiv \mathbf{J_{SQNN}}$), eq 1.[18,19]

$$\mathbf{J_{DA}} = \frac{\mathbf{H_{DA}^2} K_0}{U^2 - K_0^2} \tag{1}$$

Received: August 13, 2013
Published: October 15, 2013

   dx.doi.org/10.1021/ja4081887 | J. Am. Chem. Soc. 2013, 135, 17144–17154

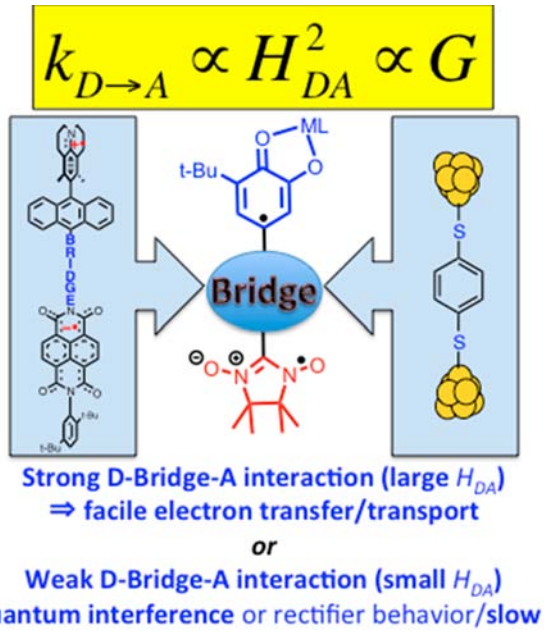

Figure 1. Cartoon suggesting the utility of D−B−A biradical electronic structure to elucidate molecular structure−property relationships in both PET reactions and conductance (**G**) in single-molecule electronic devices.

Here, $\mathbf{K_0}$ is one-half of the energy difference between the excited singlet- and triplet SQ → NN charge-transfer (CT) states and **U** is the mean CT energy. Within the VBCI model, configurational mixing between specific excited states with SQ → NN CT character and the ground state affords strong ferromagnetic coupling between the SQ and NN radicals. Variable-temperature magnetic susceptibility experiments provide $\mathbf{J_{DA}}$ as a fit parameter, while $\mathbf{K_0}$ and **U** are determined spectroscopically. In generalized D−B−A systems, low-lying D → B (electron-transfer mechanism) CT states, B → A (hole-transfer) CT states, or a combination of electron- and hole-transfer mechanisms define the nature of the superexchange pathways relative to the electronic structure of the donor, acceptor, and bridge. For photoexcited D−B−A systems or molecular wires subject to an external bias, these bridge-mediated CT processes contribute to the coherent superexchange mechanism for electron transfer and transport. Our SQ-B-NN D−B−A systems possess conjugated bridges, and we have shown that the SQ → B-NN CT state is the virtual state that figures prominently in the superexchange mechanism for magnetic exchange coupling and, for photoexcited D−B−A systems, a superexchange contribution to electron transfer.[14,18,20−24] The ability to observe the SQ → B-NN CT state directly in SQ-B-NN systems using optical spectroscopies has provided deep insight into the role of the bridge in the superexchange process.[20] Thus, within this context D−B−A biradicals provide an excellent architecture to evaluate $\mathbf{H_{DA}}$ over several orders of magnitude and for any synthetically viable bridge. In addition, since these biradical ligand complexes are quite stable, their detailed molecular structures can be probed by X-ray crystallography and conformation can be correlated with both **J** and $\mathbf{H_{DA}}$.

Oligo(*para*-phenylene)[7,25−29] and especially oligo(2,5-thiophene)[30−43] bridges are important building blocks in the continued development of molecular electronic, opto-electronic, and spintronic devices. With respect to this intense interest in oligo(*para*-phenylene) and oligo(2,5-thiophene) based materials, we have embarked on a magnetic and structural study of $\mathbf{Tp^{Cum,Me}Zn(SQ\text{-}B\text{-}NN)}$ biradical complexes containing *para*-phenylene and 2,5-thiophene bridges (B) in order to determine the distance dependence of the magnetic and electronic coupling mediated by these bridges. This is important, as there are no studies that directly compare the distance dependence of superexchange coupling and the electronic coupling matrix element ($\mathbf{H_{DA}}$) for oligo(*para*-phenylene) and oligo(2,5-thiophene) in D−B−A systems at parity of D and A. Herein, we demonstrate how a D−B−A biradical approach can be used to determine the distance dependence of $\mathbf{H_{DA}}$ for both of these important bridge moieties via direct measurement of the magnetic exchange coupling constant ($\mathbf{J_{DA}}$) by variable-temperature magnetic susceptibility measurements of the D−B−A biradical complexes **1**, **2-Ph**, **3-Ph$_2$**, **4-T**, and **5-T$_2$** depicted in Figure 2. Experimental and

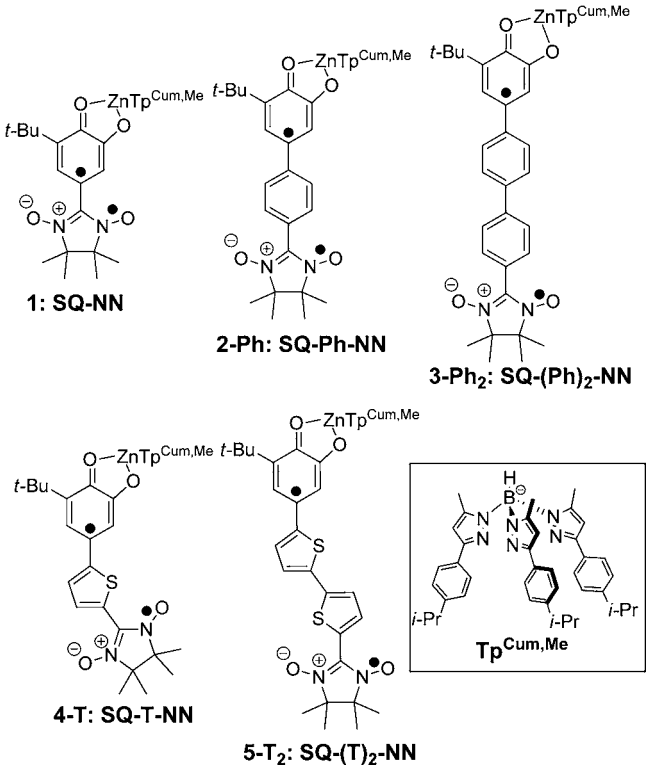

Figure 2. D−A and D−B−A biradicals studied in this work.

computational reports of HDA determination for para-phenylene[9,44,45] and for 2,5-thiophene[46,47] bridges, using both D−B−A[2] and mixed-valent[48] approaches, have appeared in the literature. However, few of these reports have the combined advantages of using a Heisenberg exchange parameter (2**J**) to compute $\mathbf{H_{DA}}$ in structurally characterized systems while avoiding categorization of the degree of delocalization in mixed-valent compounds.

RESULTS AND DISCUSSION

Synthesis of 3-Ph$_2$. As outlined in Scheme 1, aldehyde **6**[49] was reacted with CH_2I_2/I_2 to yield 4′-iodophenylbenzaldehyde **7** in excellent yield. Suzuki coupling of **7** and boronic acid **8**[50] gave protected catechol **9**. Deprotection of **9** was carried out in refluxing methanol under acidic conditions to yield catechol **10**. The aldehyde group of **10** was condensed with BHA[51] followed

dx.doi.org/10.1021/ja4081887 | J. Am. Chem. Soc. 2013, 135, 17144−17154

Scheme 1. Synthesis of 3-Ph$_2$

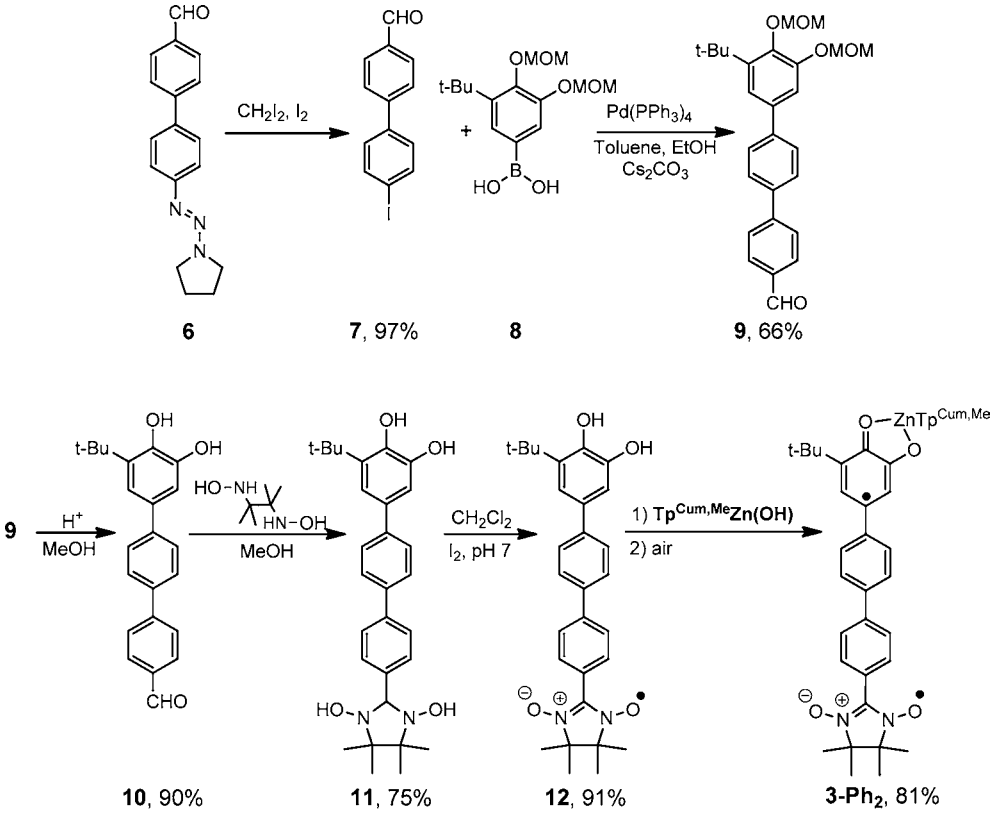

by oxidation to yield catechol-nitronylnitroxide **12**. Semiquinone biradical formation/complexation yielding **3-Ph$_2$** was effected using compound **12** and $Tp^{Cum,Me}Zn(OH)$[52] under standard conditions.[24,53,54]

Synthesis of 4-T. As outlined in Scheme 2, commercially available thiophene **13** was reacted with BHA[51] followed by oxidation to yield thiophene-nitronylnitroxide **15**. Phenol **16**, prepared by literature methods,[55] was reacted with compound **15** under Suzuki conditions to yield phenol **17**. Using IBX,[56] phenol **17** was oxidized to quinone **18**, followed by reduction to catechol **19** using ascorbic acid in pH 7 buffer. Semiquinone biradical formation of **4-T** was completed using compound **19** and $Tp^{Cum,Me}Zn(OH)$.[52]

Synthesis of 5-T$_2$. As outlined in Scheme 3, commercially available bithiophene aldehyde **20** was brominated with *N*-bromosuccinimide at low temperature to yield bithiophene bromide **21**[57] in excellent yield. Compound **21** was reacted with compound **16** under Suzuki conditions to yield phenol **22** followed by oxidation with IBX[56] giving quinone **23**. Compound **23** was reduced with ascorbic acid to yield catechol-aldehyde **24**, which was condensed with BHA[51] then oxidized to yield catechol-nitronylnitroxide **26**. Semiquinone biradical formation/complexation was completed by reacting compound **26** and $Tp^{Cum,Me}Zn(OH)$[52] under standard conditions[24,53,54] giving **5-T$_2$**.

Molecular Structures of Biradical Complexes. Thermal ellipsoid plots of complexes **1**, **2-Ph**, **3-Ph$_2$**, **4-T**, and **5-T$_2$** are shown in Figure 3 in which both hydrogen atoms and cumenyl groups were omitted for clarity. Bond lengths for *o*-SQ and NN components in each complex fall within typical values and the structural deviation parameters are summarized in Table 1. In each case, structural deviations of $\sum|\Delta_i| \approx 0.01$ Å for the *o*-SQ group and $\sum|\Delta_i| = 0.02$ Å for the NN group are small when

Scheme 2. Synthesis of 4-T

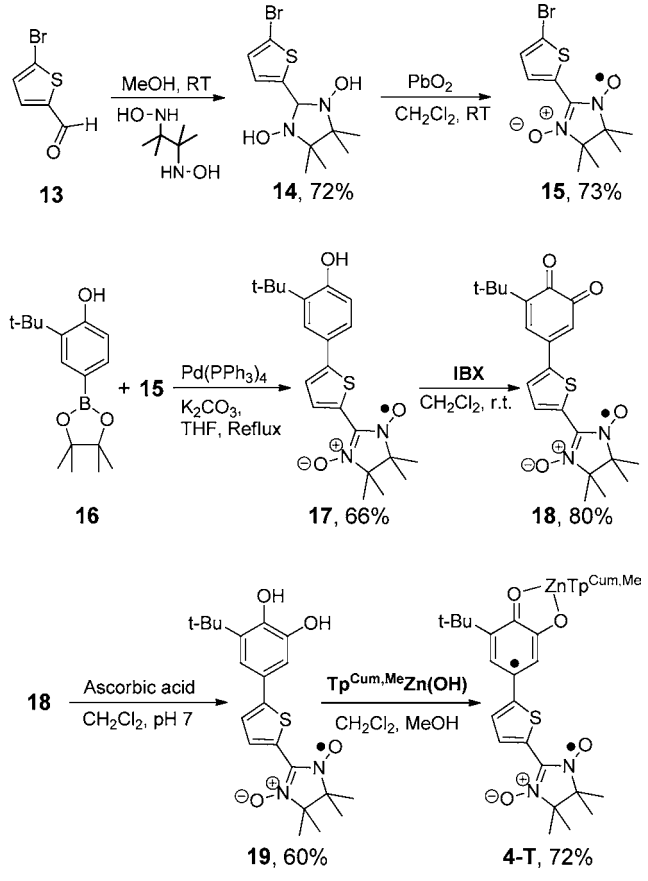

dx.doi.org/10.1021/ja4081887 | J. Am. Chem. Soc. 2013, 135, 17144−17154

Scheme 3. Synthesis of 5-T_2

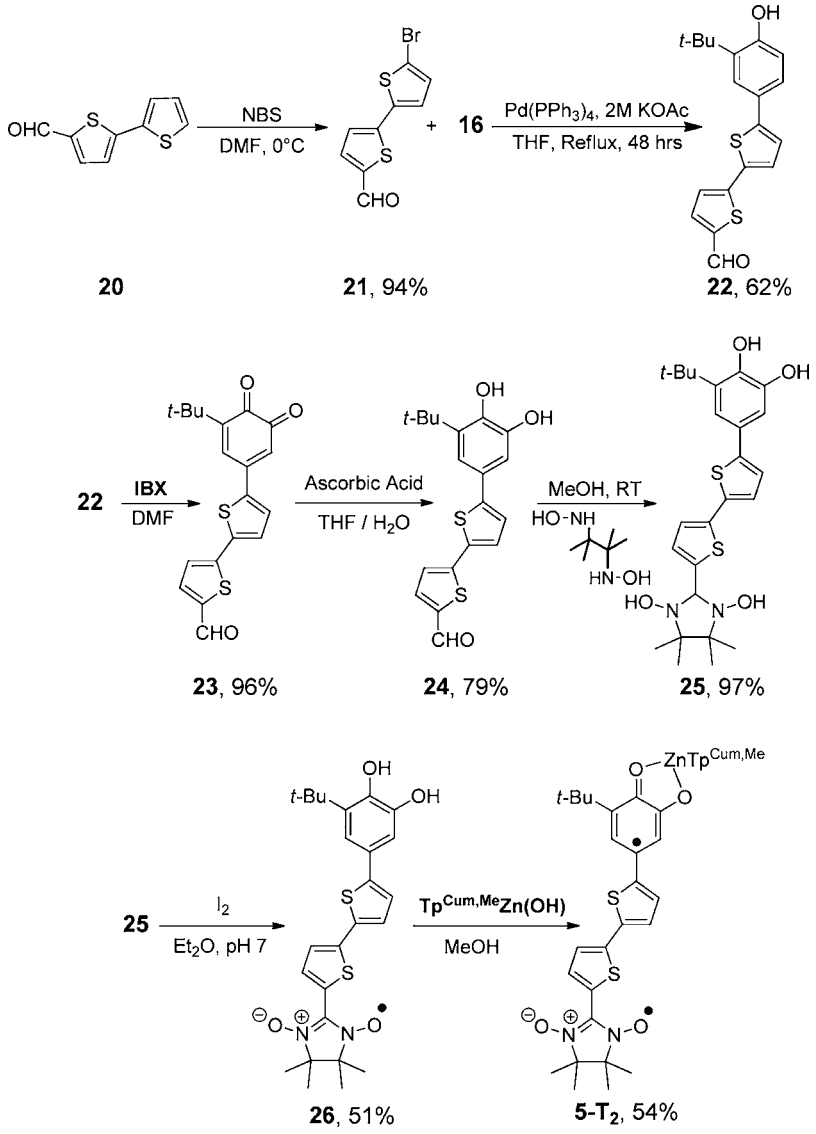

compared to previously reported semiquinone-like ligands,[54] but the ZnO_2N_3 coordination sphere is nearly identical to other $Tp^{Cum,Me}$ZnSQ-Bridge-NN complexes.[24,54,58,59] Distances between oxygen atoms on adjacent molecules, which possess appreciable spin density, on the paramagnetic nitronylnitroxide acceptors were determined to ensure the results of the magnetic susceptibility measurements (*vida infra*) reflect the intramolecular exchange coupling, J_{DA}, and not intermolecular exchange. The closest intermolecular contact for these oxygen atoms was found to be 4.691 Å for **1**, 4.861 Å for **2-Ph**, 6.088 Å for **3-Ph$_2$**, 4.604 Å for **4-T**, and 7.967 Å for **5-T$_2$**, all well outside the range for significant intermolecular contributions to the measured magnetic exchange couplings.[60−62]

Variable-Temperature Magnetic Susceptibility and Biradical Exchange Coupling. The paramagnetic susceptibility-temperature products (χ_{para}·T) for crystals of **3-Ph$_2$** and **5-T$_2$** vs temperature are shown in Figure 4. The χ_{para}·T data were fit with a simple singlet−triplet exchange model derived from the isotropic Heisenberg exchange Hamiltonian:

$$\hat{H} = -2\mathbf{J_{SQNN}}\hat{S}_{SQ}\cdot\hat{S}_{NN} \quad (2)$$

(J_{SQNN} > 0 for ferromagnetic coupling) giving a ferromagnetic J_{SQNN} = +20 cm^{-1} for **3-Ph$_2$**, and J_{SQNN} = +108 cm^{-1} for **5-T$_2$**. The downturn in the χ_{para}·T plots for T < 15K is attributed to weak intermolecular interactions and accounted for in the fit expression using a Weiss correction.

Magnetic susceptibility data (as χ_{para}·T) for **4-T** are linear suggesting Curie−Weiss behavior with J_{SQNN} > ∼250 cm^{-1}. Therefore, this required an alternate method for estimating J_{SQNN}. In cases where the spin singlet of the ferromagnetically exchange coupled biradical is not appreciably thermally populated at 300K, the exchange coupling parameter can be estimated from the ratio of the spin density (ρ) on the thiophenyl ring at the carbon attached to the NN radical to the corresponding SQ ring carbon spin density.[24,63] Since the spin densities are directly proportional to the proton hyperfine coupling constants, J_{SQNN} for **4-T** can be estimated from eq 3:[24]

dx.doi.org/10.1021/ja4081887 | J. Am. Chem. Soc. 2013, 135, 17144−17154

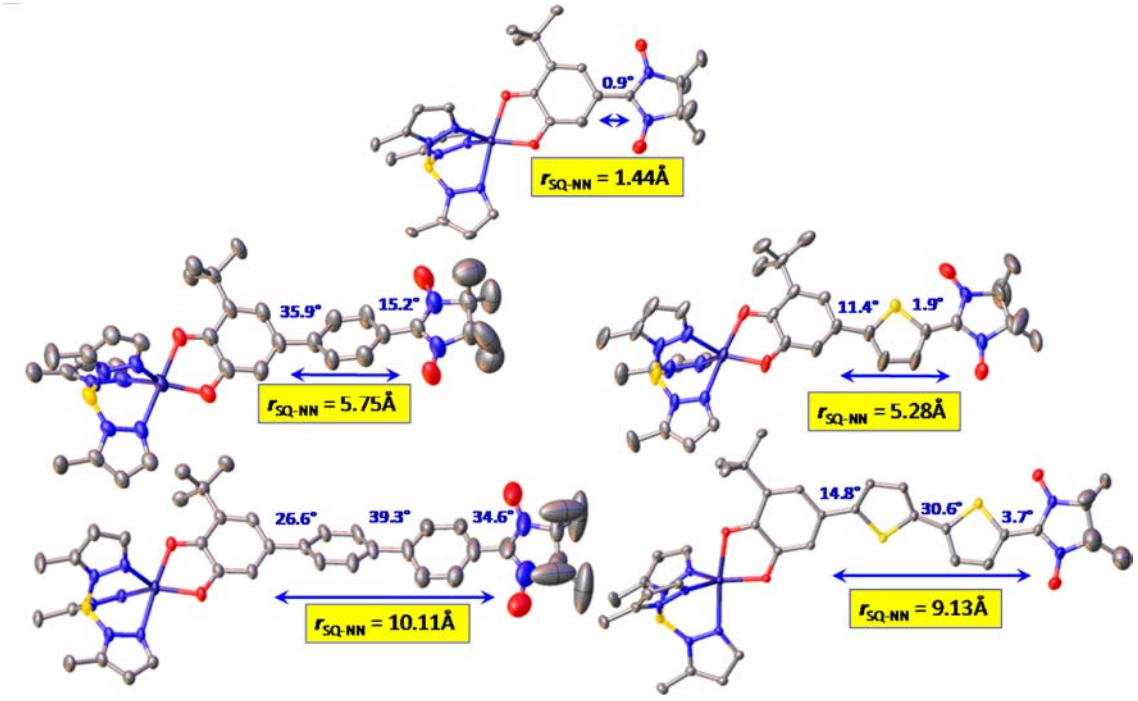

Figure 3. Thermal ellipsoid plots of complexes studied in this work. Hydrogens and cumenyl groups have been omitted for clarity. Distances are for SQ ipso-carbon to NN ipso-carbon. Angles (blue) are for torsions between adjacent ring planes.

Table 1. Structural Deviation Parameters for Complexes 1, 2-Ph, 3-Ph$_2$, 4-T, and 5-T$_2$

complex	*o*-SQ $\sum\|\Delta_i\|$ (Å)	NN $\sum\|\Delta_i\|$ (Å)
1	0.011	0.015
2-Ph	0.014	0.025
3-Ph$_2$	0.017	0.019
4-T	0.008	0.026
5-T$_2$	0.008	0.017

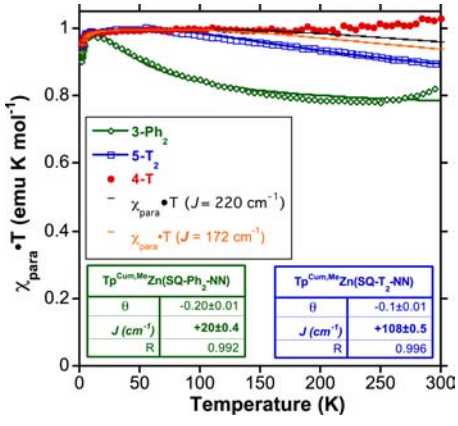

Figure 4. Plots of the paramagnetic susceptibility-temperature product (χ_{para}·T) vs temperature for **3-Ph$_2$** (green), **5-T$_2$** (blue) and **4-T** (red). Best fit lines for **3-Ph$_2$** and **5-T$_2$** are in green and blue, respectively. For **4-T**, theoretical lines correspond to **J** = +220 cm^{-1} with θ = −0.1 K (black, see text) and for **J** = +172 cm^{-1} with θ = −0.1 K (orange, see text). Insets give fit parameters (**J** = exchange parameter = one-half singlet−triplet gap and θ = Weiss correction for weak intermolecular interactions).

$$J_{SQTNN} = J_{SQNN}\left(\frac{\rho_{SQT}}{\rho_{SQ}}\right) = J_{SQNN}\left(\frac{a_{SQT}}{a_{SQ}}\right) = 550\text{cm}^{-1}\left(\frac{1.04}{3.33}\right) = 172\text{cm}^{-1} \quad (3)$$

giving J_{SQTNN} = 172 cm^{-1}. The value of **J** for **4-T** determined in this manner clearly represents a lower limit as there is no downward inflection in the experimental χ_{para}·T data (50−300K) indicating thermal population of the exchange coupled singlet state. Clearly, the experimental χ_{para}·T data (50−300K) lie above the theoretical curve for χ_{para}·T(**J** = +172 cm^{-1}) as shown in Figure 4. As such, the theoretical curve for **J** = 220 cm^{-1} was found to correlate slightly better with the experimental data below ∼220 K. Therefore, we use **J** = +220 cm^{-1} for **4-T**.

Evaluation of D−B−A Electronic Coupling Parameters. Previously, we used variable-temperature electronic absorption spectroscopy and variable-temperature magnetic susceptibility to determine H_{DA} = 10 622 cm^{-1} for **1**.[20] Thus, H_{DA} for any bridged SQ-B-NN biradical complex can be estimated from the ratio of **J** values according to eq 4:

$$\frac{J_{SQ\text{-}B\text{-}NN}}{J_{SQNN}} = \frac{H^2_{SQ\text{-}B\text{-}NN}}{H^2_{SQNN}} \quad (4)$$

Both J_{SQNN} and H_{DA} (the latter calculated using eq 4) for all complexes are given in Table 2. These data are also depicted graphically in Figure 5A,B. The values of H_{DA} for **4-T** and **5-T$_2$** reported here are within 10% of those reported by Wenger et al. for T-bridged and T$_2$-bridged mixed valence species with the caveat that they assumed Class III delocalization.[46]

We have used the plots shown in Figure 5A,B to determine the decay constant β, which describes the exponential distance

dx.doi.org/10.1021/ja4081887 | J. Am. Chem. Soc. 2013, 135, 17144−17154

Table 2. Exchange Coupling, Electronic Coupling, and D → B−A CT Energies for 1, 2-Ph, 3-Ph2, 4-T, and 5-T

complex	J_{SQNN} (cm^{-1})	$H_{DA} \equiv H_{SQNN}$ (cm^{-1})	$\Delta_{(n)}$ (cm^{-1})[c]
1[a]	550	10 622	24 650
2-Ph[a]	100	4529	22 900
3-Ph$_2$[b]	20	2015	24 200
4-T[b]	~220	~6718	21 000
5-T$_2$[b]	108	4707	19 200

[a]Ref 24. [b]This work. [c]n = number of bridge repeat units.

dependence of both the magnetic exchange coupling[64−66] and the electronic coupling matrix element[67] (eqs 5 and 6).

$$\frac{H}{H_0} = \exp\left[\frac{\beta}{2}(r - r_0)\right] \quad (5)$$

$$\frac{J}{J_0} = \exp[\beta(r - r_0)] \quad (6)$$

It is important to note that these β values were derived from compounds for which detailed electronic and molecular structure (i.e., ring conformations) information is known. This allows for further probing of the relationships that govern how geometric and electronic structure conspire to affect the distance-dependent electronic coupling as a function of bridge type. These studies are ongoing and will be the subject of future reports.

The value of β = 0.39 $Å^{-1}$ for the oligo(*para*-phenylene)-bridged SQ−B−NN species that we have determined from magnetic exchange coupling values for SQ-$(Ph)_n$-NN biradicals is quite close to that found for α,ω-oligo(*para*-phenylene)-dithiols suspended between metal contacts using conductive AFM methods (0.41 $Å^{-1}$),[68] for oligo(*para*-phenylene) bridges probed by electron transfer in a zinc(II) porphyrin system (β = 0.4 $Å^{-1}$)[69] and for oligo(*para*-phenylene) bridges in D-(*para*-$Ph)_n$-A (n = 1−5) determined from charge separation rate constants (0.46 $Å^{-1}$ for charge separation).[7]

Figure 5B shows the distance attenuation of $\mathbf{H_{ab}}$ and $\mathbf{J_{ab}}$ for the oligo(2,5-thiophene) series. The solid lines represent fits to the data using J_{SQTNN} = +220 cm^{-1} for **4-T**, while the dashed lines are fits to data using J_{SQTNN} = +172 cm^{-1} from eq 3. As is readily observed, the fits using J_{SQTNN} = +220 cm^{-1} are markedly better than those using J_{SQTNN} = +172 cm^{-1}. An internal check on the quality of the fit derives from the fact that the β values determined from fits to the electronic coupling (H/H_0) and exchange (J/J_0) parameters should be the same. This is observed for the fits using J_{SQTNN} = +220 cm^{-1} but not J_{SQTNN} = +172 cm^{-1} (Figure 5b). Thus, the β value that we determine for the oligo(2,5-thiophene)-bridged SQ-B-NN species is 0.22 $Å^{-1}$. This value for β is twice as large as that determined by break junction electrical conductance measurements on a series of oligo(2,5-thiophene) molecular wires (0.1 $Å^{-1}$) with 5, 8, 11, and 14 thiophene repeat units[70] or PET measurements of porphyrin-oligo(2,5-thiophene)-fullerene triads bridged by 4, 8, and 12 thiophene repeat units (β = 0.11 $Å^{-1}$).[71] In these studies, it was determined that the effective conjugation length was ~5 thiophene repeat units in solution. Thus, the remarkably small value for β in the PET experiments was suggested to result from highly efficient molecular wire behavior with an extraordinarily large correlation length. This discrepancy with the current work is significant and may reflect appreciable differences in how the bridge interacts with the donor and acceptor (or electrodes in transport measurements) or the onset of incoherent hopping as the dominant mechanism of transport[7] as opposed to coherent superexchange since the PET measurements show evidence for hole character on the thiophenes ($nT^{\bullet+}$).[72]

For flexible oligomeric bridges, deviations from simple exponential distance dependence of may result from conformational flexibility of the bridge.[73] However, conformational flexibility in the D−B−A molecules studied here is not an issue since the electronic coupling matrix elements ($\mathbf{H_{DA}}$) derive from an analysis of solid-state magnetic susceptibility data. More recently, it has been shown that the conductance can display a nonexponential distance dependence and even increase for bridge repeat units greater than n = 3.[74,75,33,76] This has been suggested to result from changes in the HOMO−LUMO gap that give rise to a large D−B resonance and a decrease in the energy required to remove an electron from the donor and place it on the bridge (*vide infra*). Additional contributions to β can occur in PET or biased charge-transport experiments if the bridge is capable of being

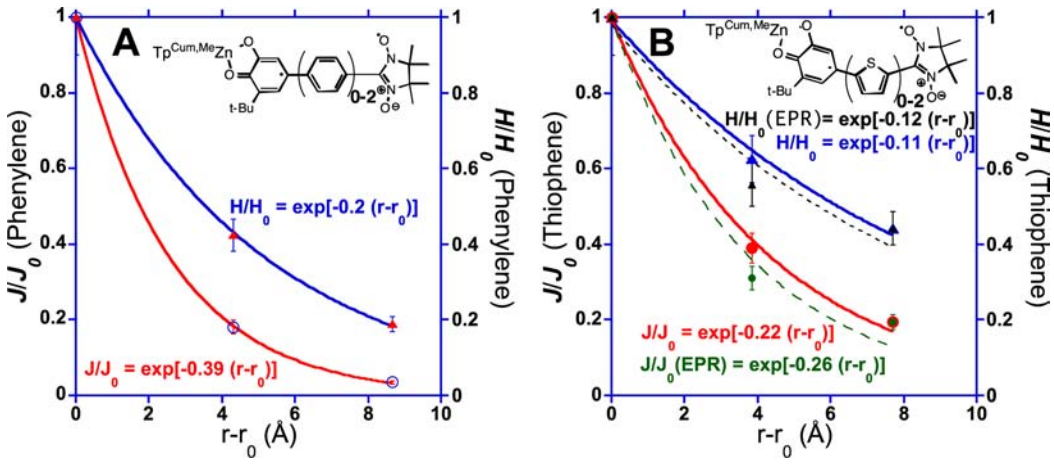

Figure 5. Exponential dependence of J_{SQNN} (red) and $\mathbf{H_{DA}}$ (blue) on distance for oligo(*para*-phenylene)-bridged biradical series, **1**, **2-Ph**, and **3-Ph$_2$** (A) and for oligo(2,5-thiophene)-bridged series, **1**, **4-T**, and **5-T$_2$** (B). Error bars correspond to propagated error in **J** values determined from multiple susceptibility experiments (see Supporting Information). The dashed lines in B represent exponential attenuation of J_{SQNN} (green) and $\mathbf{H_{DA}}$ (black) using the **J** value for **4-T** estimated from the EPR-determined ^{1}H hyperfine coupling constants (**J** = +172 cm^{-1}).

dx.doi.org/10.1021/ja4081887 | J. Am. Chem. Soc. 2013, 135, 17144−17154

oxidized or reduced. This has recently been observed by Wasielewski[7,77] where incoherent charge hopping affects the electron-transfer rate constant, indicating the molecular wire behavior in D−B−A systems does not have to derive from an energetically favorable redox gradient.

Magnetic superexchange coupling and electron-transfer/-transport phenomena are all intimately related to the electronic coupling matrix element ($\mathbf{H_{DA}}$) that connects the donor and acceptor, where the distance dependence of $\mathbf{H_{DA}}$ as a function of bridge length was given in eq 5. McConnell originally developed a second-order perturbation theory expression that relates $\mathbf{H_{DA}}$ to individual pairwise electronic coupling matrix elements between donor−bridge ($\mathbf{H_{DB}}$), bridge−bridge ($\mathbf{H_{BB}}$), and bridge−acceptor ($\mathbf{H_{BA}}$) (eq 7).[78]

$$\mathbf{H_{DA}} = \frac{\mathbf{H_{DB}}\mathbf{H_{BA}}}{\Delta}\left(\frac{\mathbf{H_{BB}}}{\Delta}\right)^{n-1} \tag{7}$$

Here, Δ is defined as the energy required to promote an electron from the donor to the bridge LUMO (electron transfer) or to promote a hole from the acceptor LUMO to bridge HOMO (hole transfer).[78] The relationship between hole and electron transfer in the D−B−A unit is depicted schematically in Figure 6.

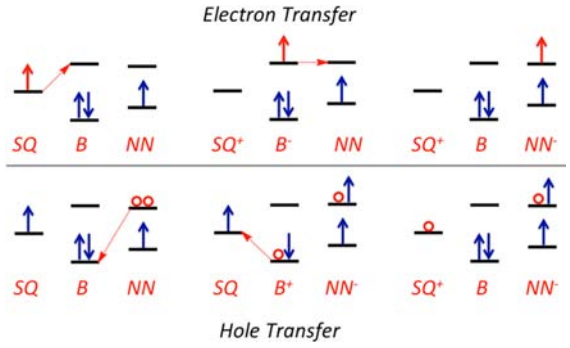

Figure 6. Relationship between CT states involving the bridge and electron-/hole-transfer mechanisms for superexchange in D−B−A systems. Here, the donor (D) is SQ, the bridge (B) is phenylene/thiophene, and the acceptor (A) is NN. Top: Electron-transfer pathway deriving from transfer of an electron from the SQ SOMO to the NN LUMO via the bridge LUMO. Bottom: Hole-transfer pathway deriving from transfer of hole from the NN LUMO to the SQ SOMO via the bridge HOMO. A low energy SQ → B−NN CT transition is observed in these $\mathbf{Tp^{Cum,Me}Zn(SQ\text{-}B\text{-}NN)}$ complexes, directly probing an electron-transfer type superexchange pathway in these molecules.

The electronic absorption spectra for these oligo(*para*-phenylene)- and oligo(2,5-thiophene)-bridged SQ-B-NN systems display intense D → B-A CT transitions in the visible region of the electronic absorption spectrum, and this excited state configurationally mixes into the ground state to promote strong ground-state ferromagnetic exchange coupling in SQ-B-NN biradicals (eq 1).[18,23] If we use the $\mathbf{H_{DA}}$ values we have determined for oligo(*para*-phenylene)- and oligo(2,5-thiophene)-bridged SQ-B-NN systems and the optical D → B-A CT energies ($\mathbf{\Delta}_n \approx \mathbf{\Delta}$) determined from electronic absorption spectroscopy, we can estimate the bridge−bridge electronic coupling matrix element, $\mathbf{H_{BB}}$. For a D−B−A system with a single bridge (n = 1) there is no $\mathbf{H_{BB}}$ term and the $\mathbf{H_{DB}H_{BA}}$ product can be determined from eq 8, where the subscript (n) denotes the number of bridge repeat units.

$$\mathbf{H_{DB}H_{BA}} = \mathbf{H_{DA(1)}}\Delta_{(1)} \tag{8}$$

This allows for a straightforward determination of $\mathbf{H_{BB}}$ using the $\mathbf{H_{DA(2)}}$ and $\mathbf{\Delta}_{(2)}$ values for the extended bridge D−B−A systems via eq 9.

$$\mathbf{H_{BB}} = \frac{\mathbf{H_{DA(2)}}\Delta_{(2)}^2}{\mathbf{H_{DA(1)}}\Delta_{(1)}} \tag{9}$$

This yields $\mathbf{H_{BB}}$ ~11 400 cm^{-1} for the Ph−Ph interaction and $\mathbf{H_{BB}}$ ~12 300 cm^{-1} for the T−T interaction, and provides a rare opportunity to compare bridge−bridge electronic coupling at parity of donor and acceptor. Within this level of approximation it becomes clear that the dominant contributor to the observed $\mathbf{H_{DA}}$ differences is not $\mathbf{H_{BB}}$ for this set of D−B−A molecules. Thus, the larger $\mathbf{H_{DA}}$ values for oligo(2,5-thiophene)- compared to oligo(*para*-phenylene)-bridged SQ-B-NN systems derive from the smaller $\mathbf{\Delta}$ values for the oligo(2,5-thiophene)s and their larger $\mathbf{H_{DB}}$ and/or $\mathbf{H_{BA}}$ values, underscoring the importance of excited-state resonant interactions between the bridge and the donor/acceptor in order to enhance the coherent superexchange mechanism for electron transfer and transport.[3] Furthermore, this highlights the importance of $\mathbf{\Delta}$ in determining $\mathbf{H_{DA}}$ and for explaining deviations from simple exponential decay laws for β that do not derive from a hopping mechanism.[74] Within the context of the McConnell model,[78] β is expected to be a function of $\mathbf{\Delta}$, $\mathbf{H_{BB}}$, and the length of the bridge repeat unit, R_0 according to eq 10.

$$\beta = \frac{2}{R_0}\ln\left|\frac{\Delta}{\mathbf{H_{BB}}}\right| \tag{10}$$

Given the experimentally determined $\mathbf{\Delta}_{(n)}$, $\mathbf{H_{BB}}$, and R_0 values for these D−B−A systems, the dominant contributor to differences in oligo(*para*-phenylene) and oligo(2,5-thiophene) β values appears to be $\mathbf{\Delta}$. This is in agreement with the computational analysis of Eng and Albinsson,[74] who noted that β is not specifically related to the nature of the bridge but is rather a property of the entire D−B−A ensemble. A simple relationship has also been derived that relates β to the effective barrier height (ΔE_{eff}) for an electron tunneling through a square potential barrier (eq 11):[79,80]

$$\Delta E_{\text{eff}} = \left(\frac{\hbar^2}{8m_e}\right)\beta^2 = (0.952\text{eV} \times \text{Å}^2)\beta^2 \tag{11}$$

where m_e is the mass of the tunneling electron. Using the experimentally derived β values from the oligo(*para*-phenylene)-bridged biradical series, **2-Ph**, and **3-Ph$_2$** and the oligo(2,5-thiophene)-bridged series, **4-T** and **5-T$_2$**, this results in ΔE_{eff} = 1168 and 372 cm^{-1}, respectively. Thus, the effective barrier height for oligo(*para*-phenylene) is approximately three times greater than that for oligo(2,5-thiophene). In summary, the observed dependence of $\mathbf{H_{DA}}$ on the $\mathbf{H_{DB}H_{BA}}$ product and $\mathbf{\Delta}$ clearly highlights the need for detailed spectroscopic studies of structurally characterized D−B−A systems in order to fully understand excited-state electronic structure contributions to long-range electronic coupling and coherent electron-transfer/-transport behavior as a function of donor, acceptor, and bridge.

■ CONCLUSIONS

A combination of variable-temperature magnetic susceptibility measurements, hyperfine couplings, and X-ray crystal structures have allowed us to determine the exchange and electronic

coupling exponential decay constants for two quintessential bridges: oligo(*para*-phenylene), β = 0.39 Å^{-1} and oligo(2,5-thiophene), β = 0.22 Å^{-1}. Thus, β for oligo(2,5-thiophene) is twice the β value we determine for oligo(*para*-phenylene). This report represents the first direct comparison of exchange/electronic coupling and distance dependence for these bridges.

Our experimentally derived relationships between β and $\mathbf{H_{DA}}$ are from direct measurement of the isotropic exchange coupling constant ($\mathbf{J}$) determined as a fit parameter to variable-temperature magnetic susceptibility data. These studies also represent the direct measurement of superexchange contributions to β, with no contribution from incoherent hopping. Since the attenuation factor is solely due to superexchange, the key factors affecting β can be evaluated. We determined that the difference in β for oligo(*para*-phenylene) and oligo(2,5-thiophene) is due primarily to the D−B energy gap, $\mathbf{\Delta}$, rather than bridge−bridge electronic couplings, $\mathbf{H_{BB}}$. This conclusion is supported by estimating values for $\mathbf{H_{BB}}$ from eqs 8 and 9: $\mathbf{H_{BB}}$ = 11 400 cm^{-1} for oligo(*para*-phenylene) and $\mathbf{H_{BB}}$ = 12 300 cm^{-1} for oligo(2,5-thiophene) where it is clear that an 8% difference in $\mathbf{H_{BB}}$ cannot account for a factor of ∼2 in the calculated β values. The results presented here offer unique insight into the intrinsic molecular factors that govern $\mathbf{H_{DA}}$ and β and are important for understanding the electronic origin of facile electron-transfer and electron-transport behavior involving molecular bridges.

EXPERIMENTAL SECTION

General Considerations. Reagents and solvents were purchased from commercial sources and used as received unless otherwise noted. ^{1}H and ^{13}C NMR spectra were recorded on either a Varian Mercury 300 MHz or a Varian Mercury 400 MHz spectrometer at room temperature. ^{1}H and ^{13}C chemical shifts are listed in parts per million (ppm) and are referenced to residual protons or carbons of the deuterated solvents, respectively. Infrared spectra were recorded on a Brüker Vertex 80v spectrometer with Brüker Platinum ATR attachment. Electronic absorption spectra were collected on a Shimadzu UV-1601 UV−vis spectrophotometer. EPR spectra were collected on an IBM Instruments ER-200D-SRC spectrometer. Microcrystalline samples of ∼2 mM concentration were prepared in tetrahydrofuran and freeze−pump−thawed several times, and the spectra were simulated using WinSIM. Elemental analyses were performed by Atlantic Microlabs, Inc. High-resolution mass spectra were obtained at the NCSU Department of Chemistry Mass Spectrometry Facility and the Duke University Department of Chemistry Mass Spectrometry Facility. Compounds **1**,[54] **2-Ph**,[24] **6**,[49] **8**,[50] **16**,[55] **21**[57] *o*-iodoxybenzoic acid (**IBX**),[56] 2,3-dimethyl-2,3-bis(hydroxyamino)butane (**BHA**),[51] and $\mathbf{Tp^{Cum,Me}Zn(OH)}$[44] were synthesized as previously described. Compounds **3-Ph$_2$**, **4-T**, and **5-T$_2$** were prepared as outlined below.

Magnetometry. Magnetic susceptibility and saturation plots were performed on a Quantum Design MPMS-XL SQUID magnetometer. Microcrystalline samples of ∼15 mg were loaded into gelcap/straw holders and mounted to the sample rod with Kapton tape for susceptibility experiments. Raw susceptibility data were collected with an applied field of 0.7 T and corrected for diamagnetic response of the sample using Pascal's constants as a first approximation, with a separate diamagnetic correction for the sample holder.

X-ray Diffraction. Information including the experimental details of the structural determination of the new metal complexes in this work can be found in the Supporting Information.

4′-Iodo-[1,1′-biphenyl]-4-carboxaldehyde (7). A 50 mL Schlenk flask containing **6** (500 mg, 1.79 mmol), iodine (453 mg, 1.79 mmol) and CH_2I_2 (8 mL) was degassed by 4 freeze−pump−thaw cycles. The reaction mixture was heated at 100 °C for 4 h. Diiodomethane was removed under reduced pressure. The residue was dissolved in $CHCl_3$, washed with a saturated solution of Na_2SO_3 and brine, dried with sodium sulfate, filtered, and evaporated to dryness. The solid residue was purified by recrystallization from CH_2Cl_2/hexanes mixed solvent to afford **7** as a brown solid (550 mg, 97%). ^{1}H NMR (300 MHz, $CDCl_3$, δ): 10.06 (s, 1H), 7.96 (d, J = 8.3 Hz, 2H), 7.82 (d, J = 8.3 Hz, 2H), 7.72 (d, J = 8.3 Hz, 2H), 7.37 (d, J = 8.3 Hz, 2H). ^{13}C NMR (75 MHz, $CDCl_3$) δ (ppm): 191.9, 146.0, 139.3, 138.3, 135.6, 130.6, 129.2, 127.5, 94.7. IR (solid) ν_{max} (cm^{-1}): 3056, 2922, 2822, 2727, 1692, 1600, 1572, 1547, 1475, 1417, 1383, 1306, 1286, 1258, 1208, 1164, 1104, 1062, 908, 840, 806. Mass spectrometry (m/z): 308.9763 (M + H)$^+$.

3″-(*tert*-Butyl)-4″,5″-bis(methoxymethoxy)-[1,1′:4′,1″-terphenyl]-4-carboxaldehyde (9). To a 50 mL Schlenk flask,7 (440 mg, 1.38 mmol), **8** (500 mg, 1.50 mmol), $Pd(PPh_3)_4$ (79.0 mg, 0.0684 mmol), cesium carbonate (890 mg, 2.73 mmol), and ethanol (5 mL) in dried toluene (10 mL) were added, placed under a nitrogen atmosphere, and refluxed for 48 h. After the reaction mixture was cooled to room temperature, 20 mL water was added, and stirred for 30 min. The resulting mixture was filtered through Celite, and the solvent removed under reduced pressure. The residue was extracted using CH_2Cl_2, washed with a saturated sodium bicarbonate solution followed by brine, dried with sodium sulfate, filtered, and concentrated *in vacuo*. The solid residue was purified by column chromatography (4:1 hexanes:ethyl acetate) to provide **9** as brown oil (440 mg, 66%). ^{1}H NMR (300 MHz, $CDCl_3$, δ): 10.07 (s, 1H), 7.97 (d, J = 8.3 Hz, 2H), 7.80 (d, J = 8.3 Hz, 2H), 7.71 (d, J = 8.3 Hz, 2H), 7.67 (d, J = 8.3 Hz, 2H), 7.31 (s, 1H), 7.28 (s, 1H), 5.27 (s, 2H), 5.26 (s, 2H), 3.68 (s, 3H), 3.53 (s, 3H), 1.49 (s, 9H). ^{13}C NMR (75 MHz, $CDCl_3$, δ): 192.0, 150.6, 146.8, 146.0, 143.9, 141.6, 138.3, 135.4, 135.3, 130.5, 127.8, 127.6, 119.5, 113.5, 99.2, 95.6, 57.8, 56.5, 35.5, 30.7. IR (thin film) ν_{max} (cm^{-1}): 2955, 2900, 2822, 2727, 1700, 1602, 1571, 1551, 1524, 1471, 1435, 1391, 1360, 1324, 1264, 1233, 1213, 1162, 1077, 1030, 1007, 958, 880, 840, 818. Mass spectrometry (m/z): 457.1975 (M + Na)$^+$.

3″-(*tert*-Butyl)-4″,5″-dihydroxy-[1,1′:4′,1″-terphenyl]-4-carboxaldehyde (10). To a 50 mL round-bottom flask containing **9** (350 mg, 0.806 mmol) in methanol (3 mL) was added 3 drops of 12 M HCl and 1 drop of water, and the solution was refluxed overnight. The solvent was removed under reduced pressure, and the crude reaction mixture was extracted using CH_2Cl_2, washed with brine. The organic phase was then dried with sodium sulfate, filtered, and concentrated *in vacuo*. The solid was recrystallized from a mixture of methanol and diethyl ether to provide **10** as a light-orange solid (250 mg, 90%). ^{1}H NMR (300 MHz, DMSO-d_6, δ): 10.06 (s, 1H), 9.61 (s, 1H), 8.29 (s, 1H), 8.01 (d, J = 8.3 Hz, 2H), 7.95 (d, J = 8.3 Hz, 2H), 7.82 (d, J = 8.3 Hz, 2H), 7.64 (d, J = 8.3 Hz, 2H), 7.02 (s, 1H), 6.98 (s, 1H), 1.40 (s, 9H). ^{13}C NMR (75 MHz, $CDCl_3$, δ): 192.7, 145.5, 144.3, 141.4, 136.4, 136.0, 135.0, 130.2, 129.2, 127.6, 127.0, 126.7, 115.6, 111.2, 34.5, 29.4. IR (solid) ν_{max} (cm^{-1}): 3489, 3417, 2956, 1664, 1600, 1571, 1488, 1435, 1400, 1373, 1358, 1300, 1286, 1218, 1190, 1169, 1151, 1108, 1068, 1003, 947, 875, 842, 813, 766, 753. Mass spectrometry (m/z): 369.1458 (M + Na)$^+$.

2-(3″-(*tert*-Butyl)-4″,5″-dihydroxy-[1,1′:4′,1″-terphenyl]-4-yl)-4,4,5,5-tetramethylimidazolidine-1,3-diol (11). A 10 mL Schlenk flask containing **10** (100 mg, 0.290 mmol) and BHA (90.0 mg, 0.600 mmol) with a minimal amount of methanol was pump/purged with nitrogen and then stirred at room temperature for 48 h. The reaction was filtered and washed with cold methanol to yield **11** as a white solid (100 mg, 75%). ^{1}H NMR (300 MHz, DMSO-d_6, δ): 9.57 (s, 1H), 8.22 (s, 1H), 7.79 (s, 2H), 7.68 (d, J = 8.1 Hz, 2H), 7.63 (d, J = 8.1 Hz, 2H), 7.57 (s, 2H), 6.98 (s, 1H), 6.94 (s, 1H), 4.55 (s, 1H), 1.40 (s, 9H), 1.09 (s, 6H) 1.07 (s, 6H). ^{13}C NMR (75 MHz, $CDCl_3$, δ): 145.5, 144.0, 141.2, 140.1, 138.9, 138.1, 136.0, 129.7, 129.1, 127.0, 126.5, 125.7, 115.5, 111.2, 90.1, 66.1, 54.9, 34.5, 29.4, 24.4, 17.2. IR (solid) ν_{max} (cm^{-1}): 3524, 3222, 2950, 2901, 1604, 1484, 1435, 1392, 1367, 1319, 1250, 1200, 1150, 1111, 1092, 1069, 947, 915, 875, 822, 769, 753, 722. Mass spectrometry (m/z): 477.2741 (M + H)$^+$.

2-(3″-(*tert*-Butyl)-4″,5″-dihydroxy-[1,1′:4′,1″-terphenyl]-4-yl)-4,4,5,5,-tetramethyl-4,5-dihydroimidazol-3-oxide-1-oxyl (12). A 100 mL round-bottom flask containing **11** (50.0 mg, 0.108

dx.doi.org/10.1021/ja4081887 | J. Am. Chem. Soc. 2013, 135, 17144−17154

mmol) in CH_2Cl_2, pH 7 buffer, and cetyltrimethyl ammonium bromide (10.0 mg, 0.0274 mmol) was cooled to 0 °C. Iodine (43.2 mg, 0.170 mmol) in CH_2Cl_2 was added dropwise at 0 °C. The mixture was stirred at 0 °C for an additional 30 min. The organic layer was separated and washed with a saturated solution of sodium thiosulfate and brine. The organic phase was then dried with sodium sulfate, filtered, and concentrated *in vacuo*. The solid residue was purified by recrystallization from CH_2Cl_2/hexanes mixed solvent to provide **12** as a blue-green solid (45.5 mg, 91%). IR (solid) ν_{max} (cm^{-1}): 3505, 3195, 2925, 2850, 1653, 1603, 1536, 1483, 1422, 1387, 1361, 1322, 1311, 1254, 1215, 1165, 1133, 1106, 1070, 955, 872, 822, 800, 736, 699, 618, 540. EPR (CH_2Cl_2, 298 K) a_N = 7.64 G. Mass spectrometry (m/z): 472.2353 $(M - H)^-$.

$Tp^{Cum,Me}$Zn(SQ-Ph-Ph-NN) (3-Ph_2). A 25 mL Schlenk flask containing **12** (50.0 mg, 0.108 mmol), **$Tp^{Cum,Me}$Zn(OH)** (75.0 mg, 0.108 mmol), and 10 mL of 1:1 methanol/CH_2Cl_2 was pump/purged with nitrogen then stirred under N_2 at room temperature for 1 h and opened to air overnight. The brown precipitate was collected and dried under vacuum. The solid was recrystallized from a CH_2Cl_2/methanol solution to yield **3-Ph_2** as a brown solid (100 mg, 81%). IR (solid) ν_{max} (cm^{-1}): 2954, 2921, 2850, 2540, 1605, 1575, 1550, 1519, 1463, 1439, 1386, 1361, 1258, 1172, 1094, 1061, 983, 821, 788, 746, 644. EPR (CH_2Cl_2, 298 K) a_N = 3.92 G. Elemental Analysis: calcd (C: 71.23, H: 6.77, N: 9.77); found: (C: 70.79, H: 6.94, N: 9.41).

2-(5′-Bromothiophen-2-yl)-4,4,5,5-tetramethylimidazolidine-1,3-diol (14). In a 20 mL vial **13** (1.33 g, 6.96 mmol) was added with **BHA** (1.01 g, 6.82 mmol), and the solids were dissolved in 10 mL distilled methanol. The reaction was purged with N_2 and stirred for 24 h. The precipitate formed was collected yielding pure white **14** (1.57 g, 72%). ^{1}H NMR (300 MHz, DMSO-d_6, δ): 8.02 (s, 2H), 7.05 (d, J = 3.91 Hz, 1H), 6.90 (d, J = 3.9 Hz, 1H), 4.28 (s, 1H), 1.03 (s, 6H), 1.015 (s, 6H).

2-(5-Bromothiophen-2-yl)-4,4,5,5,-tetramethyl-4,5-dihydroimidazol-3-oxide-1-oxyl (15). To a 100 mL round-bottom flask containing **14** (1.15 g, 3.58 mmol) and 40 mL distilled methanol, an excess of lead(IV) oxide was added and left to stir. After 30 min thin-layer chromatography (TLC) (100% ethyl acetate) showed **15** (ΔR_f = 0.45, deep blue) and **14** (ΔR_f = 0.11, colorless, UV active). After 1 h total reaction time no starting material was present. The reaction was filtered, and solvent removed under reduced pressure. The product was purified by radial chromatography (gradient, 100% hexanes → 20% ethyl acetate in hexanes) yielding a pure blue solid, **15** (0.830 g, 73%) EPR (X-band, 298 K): pentet, a_N = 7.71 G. IR (thin film) ν_{max} (cm^{-1}): 2998, 1431, 1401, 1368, 1199, 1141, 793.

2-(5-(3-(*tert*-Butyl)-4-hydroxyphenyl)thiophen-2-yl)-4,4,5,5,-tetramethyl-4,5-dihydroimidazol-3-oxide-1-oxyl (17). A 100 mL Schlenk flask was charged with **15** (0.288 g, 1.04 mmol), **16** (0.366, 1.15 mmol), and $Pd(PPh_3)_4$ (65 mg, 0.0562 mmol). The Schlenk flask was sealed and pump/purged 3 times. Thirty mL of dry, degassed THF was then added along with 1.8 mL 2 M potassium carbonate. A reflux condenser was fit, the reaction freeze−pump−thawed 3 times, and the reaction was refluxed for 48 h. The reaction mixture was allowed to cool to room temperature, washed with H_2O, and filtered through a silica plug. The solvent was removed, and the product was purified by column chromatography (98% CH_2Cl_2, 2% methanol yielding 0.268 g (0.692 mmol, 66%) of **17** as a green solid. EPR (X-band, 298K): pentet, a_N = 7.50 G. IR (solid) ν_{max} (cm^{-1}): 2969, 2913, 2856, 2538, 1525, 1431, 1356, 1169, 1056, 831, 794, 644, 540. UV (CH_2Cl_2) λ_{max}, nm (ε): 351 (44391), 624 (487), 686 (697), 759 (453).

3-(*tert*-Butyl)-5-(5-(1,3-dihydroxy-4,4,5,5,-tetramethyl-4,5-dihydroimidazol-3-oxide-1-oxyl)thiophen-2-yl)cyclohexa-3,5-diene-1,2-dione (18). Phenol **17** (0.200 g, 0.516 mmol) was dissolved in 10 mL of CH_2Cl_2 and 10 mL methanol. **IBX** (0.87 g, 3.11 mmol) was added, the reaction turned dark red within 30 min, and reacted for 16 h. The solvent was removed and the product was purified by column chromatography (50:50 hexanes/ethyl acetate) yielding 0.165 g (0.411 mmol, 80%) of **18** as a dark red solid. EPR (X-band, 298K): pentet, a_N = 7.81 G. IR (solid) ν_{max} (cm^{-1}): 2931, 2858, 1637, 1618, 1543, 1375, 1243, 1131, 812, 737. UV (CH_2Cl_2) λ_{max}, nm (ε): 312 (10281), 486 (4705)

2-(5-(3-(*tert*-Butyl)-4,5-dihydroxyphenyl)thiophen-2-yl)-4,4,5,5,-tetramethyl-4,5-dihydroimidazol-3-oxide-1-oxyl (19). A 100 mL Schlenk flask was charged with (212 mg, 0.528 mmol) **18** and 30 mL CH_2Cl_2 and the solution was freeze−pump−thawed three times. A degassed solution of ascorbic acid (93 mg, 52.8 mmol) in 30 mL of 0.1 M pH 7 buffer solution was added to the reaction mixture. The reaction stirred for 3 h and monitored by TLC. The organic layer was removed via syringe and placed into an evacuated 50 mL round-bottom flask where all but 5 mL of solvent was removed. Thirty mL of petroleum ether was added and the product was placed in a −15 °C freezer to precipitate. After 24 h a green precipitate was collected by vacuum filtration yielding 127 mg (0.314 mmol, 60%) of **19**. EPR (X-band, 298K): pentet, a_N = 7.54 G. IR (thin film) ν_{max} (cm^{-1}): 3175, 2955, 1600, 1431, 1356, 1289, 1207, 1131, 1066, 948, 793, 531. UV (CH_2Cl_2) λ_{max}, nm (ε): 355 (16374), 678 (295).

$Tp^{Cum,Me}$Zn(5-SQ-thiophen-2-yl-NN) (4-T). A dry 50 mL Schlenk flask was filled with **19** (97 mg, 0.240 mmol) and **$Tp^{Cum,Me}$Zn(OH)** (165 mg, 0.238 mmol) and pump/purged with nitrogen several times. A mixture of 25 mL CH_2Cl_2 and 15 mL methanol were degassed and then transferred into the Schlenk flask. The reaction mixture immediately turned dark brown upon addition of the solvent and stirred under nitrogen for 12 h. The reaction mixture was then exposed to air and the monitored by EPR. After 24 h, the solvent was removed under reduced pressure and the product was purified by column chromatography (100% CH_2Cl_2,basic alumina) yielding 186 mg (0.172 mmol, 72%) of **4-T** as a brown solid. The product was crystallized by slow evaporation of methanol. EPR (X-band, 298K): pentet, apparent a_N = 3.96 G. IR (solid) ν_{max} (cm^{-1}): 2969, 2913, 2856, 2538, 1525, 1431, 1356, 1169, 1056, 831, 794, 644, 540. UV (CH_2Cl_2) λ_{max}, nm (ε): 386 (4863), 445 (10659), 475 (12325), 860 (467).

5′-Bbromo-[2,2′-bithiophene]-5-carbaldehyde (21).[57] To a 15 mL round-bottom flask, 557 mg (2.87 mmol) [2,2′-bithiophene]-5-carbaldehyde was added with 515 mg (2.89 mmol) NBS in 1.5 mL DMF and stirred at −10 °C in the dark for 18 h. The reaction mixture was poured into 100 mL deionized water and stirred for 5 min after which a white solid precipitates and was collected via vacuum filtration to yield 738 mg (94%) of compound **21**. ^{1}H NMR (300 MHz, $CDCl_3$) δ: 9.87 (s, 1H), 7.66 (d, J = 3.9 Hz, 1H), 7.18 (d, J = 3.9 Hz, 1H), 7.11 (d, J = 3.9 Hz, 1H), 7.04 (d, J = 3.9 Hz, 1H).

5′-(3-(*tert*-Butyl)-4-hydroxyphenyl)-[2,2′-bithiophene]-5-carboxaldehyde (22). To a 100 mL oven-dried Schlenk flask, 641 mg (2.32 mmol) **16**, 624 mg (2.29 mmol) **21**, and 150 mg (0.13 mmol) $Pd(PPh_3)_4$ were added with ∼15 mL tetrahydrofuran under a nitrogen atmosphere. A 2 M K_2CO_3 solution was degassed with nitrogen, and 4 mL (8 mmol) was added to the reaction vessel by purged syringe. The reaction flask was fit with a condenser, refluxed for 2 days, and checked by TLC (75% ethyl acetate in hexanes) to ensure product formation. After the reaction was cooled to room temperature, ∼30 mL deionized water was added, and the mixture stirred in air for 30 min. The mixture was then transferred to a separatory funnel, diluted with 100 mL ethyl acetate, and washed twice with a saturated sodium chloride solution. The organic layer was dried over sodium sulfate, and the solvent removed under reduced pressure. The resulting brown oil was purified by column chromatography (20% ethyl acetate in hexanes) to yield 484 mg (62%) of compound **22**. ^{1}H NMR (400 MHz, DMSO-d_6, δ): 9.87 (s, 1H), 9.82 (s, 1H), 7.98 (d, J = 3.9 Hz, 1H), 7.56 (d, J = 3.9 Hz, 1H), 7.52 (d, J = 3.9 Hz, 1H), 7.39 (m, 3H), 6.85 (d, J = 8.19 Hz, 1H), 1.38 (s, 9H). ^{13}C NMR (100 MHz, DMSO-d_6) δ (ppm): 184.25, 157.36, 147.37, 146.58, 141.47, 139.81, 136.84, 133.16, 128.82, 125.25, 125.14, 124.72, 123.90, 117.60, 35.05, 29.90. IR (solid) ν_{max} (cm^{-1}): 3330 (br, O−H), 1640 (s, C═O). Elemental Analysis: calcd: (C: 66.63, H: 5.30); found: (C: 66.75, H: 5.38).

5′-(5-(*tert*-Butyl)-3,4-dioxocyclohexa-1,5-dien-1-yl)-[2,2′-bithiophene]-5-carboxaldehyde (23). To a 50 mL round-bottom flask, 230 mg (0.67 mmol) **22** and 376 mg (1.34 mmol) **IBX** were added with 2 mL *N*,*N*-dimethylformamide. The reaction was covered with aluminum foil and stirred in air for 20 h. After ensuring all of the

dx.doi.org/10.1021/ja4081887 | J. Am. Chem. Soc. 2013, 135, 17144−17154

starting material was consumed, the reaction was poured into 50 mL deionized water and diluted with ethyl acetate. The mixture was transferred to a separatory funnel and washed twice with saturated sodium bicarbonate followed by two washes of saturated sodium chloride. The organic layer was collected and dried over sodium sulfate, and the solvent removed under reduced pressure to yield 228 mg (96%) of dark red compound **23**. ^{1}H NMR (400 MHz, $CDCl_3$, δ): 9.92 (s, 1H), 7.74 (d, J = 4.0 Hz, 1H), 7.59 (d, J = 4.0 Hz, 1H), 7.44 (d, J = 4.0 Hz, 1H), 7.41 (d, J = 4.0 Hz, 1H), 7.22 (d, J = 2.2 Hz, 1H), 6.64 (d, J = 2.2 Hz, 1H), 1.35 (s, 9H). ^{13}C NMR (100 MHz, $CDCl_3$) δ (ppm): 182.28, 179.77, 179.58, 151.84, 144.79, 143.61, 143.10, 141.71, 141.27, 136.78, 132.06, 130.23, 127.49, 126.02, 120.03, 35.85, 29.20. IR (solid) ν_{max} (cm^{-1}): 1658 (s, C═O), 1645 (s, C═O), 1637 (s, C═O). Mass spectrometry (m/z): 357.0610 (M + H)$^+$.

5′-(3-(*tert*-Butyl)-4,5-dihydroxyphenyl)-[2,2′-bithiophene]-5-carboxaldehyde (24). The dark red quinone, **23** (228 mg, 0.64 mmol), was dissolved in 10 mL tetrahydrofuran and transferred to a separatory funnel. In a 125 mL Erlenmeyer flask, 125 mg (0.70 mmol) ascorbic acid was dissolved in 10 mL deionized water and added to the separatory funnel containing **23**. Upon shaking the mixture, the dark red color faded to a light yellow. To separate the layers, 100 mL saturated sodium chloride solution was added, and the organic layer was diluted with 50 mL ethyl acetate. The organic layer was then washed twice with saturated sodium chloride solution, dried over $MgSO_4$, and the solvent removed under reduced pressure to yield 181 mg (79%) of compound **24**. ^{1}H NMR (400 MHz, DMSO-d_6, δ): 9.87 (s, 1H), 9.75 (s, 1H), 8.52 (s, 1H), 7.99 (d, J = 4.0 Hz, 1H), 7.55 (d, J = 4.0 Hz, 1H), 7.52 (d, J = 4.0 Hz, 1H), 7.28 (d, J = 4.0 Hz, 1H), 6.99 (d, J = 2.0 Hz, 1H), 6.96 (d, J = 2.0 Hz, 1H), 1.37 (s, 9H). ^{13}C NMR (100 MHz, DMSO-d_6) δ (ppm): 183.44, 146.80, 145.74, 145.43, 144.95, 140.64, 139.03, 136.27, 132.29, 127.98, 124.45, 122.92, 122.85, 114.81, 110.22, 34.29, 29.18. IR (solid) ν_{max} (cm^{-1}): 3090 (br, OH), 1625 (s, C═O). Mass spectrometry (m/z): 359.0768 (M + H)$^+$.

2-(5′-(3-(*tert*-Butyl)-4,5-dihydroxyphenyl)-[2,2′-bithiophen]-5-yl)-4,4,5,5-tetramethylimidazolidine-1,3-diol (25). To a 5 mL round-bottom flask, 101 mg (0.28 mmol) **24** was added with 84 mg (0.57 mmol) **BHA** and a magnetic stir bar. The flask is sealed with a rubber septum, attached to a Schlenk line, and pump/purged with nitrogen 5 times. Using a purged syringe, 2 mL of distilled and degassed methanol was added and heated gently to dissolve the contents of the flask. The reaction was stirred in the dark, under nitrogen, for 2 days and checked for completion by ^{1}H NMR. With an absence of a signal for the aldehyde proton of **24**, the reaction is stopped by removing the solvent under reduced pressure, and the crude product **25** (133.8 mg, 97%) is used directly in the synthesis of compound **26**. IR (solid) ν_{max} (cm^{-1}): 3250 (br, OH and NH).

2-(5′-(3-(*tert*-Butyl)-4,5-dihydroxyphenyl)-[2,2′-bithiophen]-5-yl)-4,4,5,5,-tetramethyl-4,5-dihydroimidazol-3-oxide-1-oxyl (26). To a 100 mL round-bottom flask, 142 mg (0.29 mmol) **25** was dissolved in 30 mL diethyl ether and 10 mL freshly prepared buffer (pH 7). In a 125 mL separatory funnel, 119 mg (0.47 mmol) sublimed iodine was dissolved in 30 mL diethyl ether. The reaction flask was chilled to 0 °C, and the solution of iodine was added dropwise with stirring. Once all of the iodine was added, the reaction was warmed to room temperature, and 100 mL buffer (pH 7) was added. The reaction was transferred to a separatory funnel and washed with a saturated sodium thiosulfate solution followed by two washes of saturated sodium chloride. The organic layer was collected, dried over $MgSO_4$, and the solvent removed under reduced pressure to yield 73 mg (51%) of compound **26**. IR (solid) ν_{max} (cm^{-1}): 3070 (br, OH). EPR (X-Band, 298 K): pentet (1:2:3:2:1), a_N = 7.8 G.

Tp^{Cum,Me}Zn(5′-SQ-[2,2′-bithiophen]-5-yl-NN) (5-T$_2$). To an oven-dried 25 mL Schlenk flask, 70 mg (0.14 mmol) **26** was added with 146 mg (0.21 mmol) **Tp^{Cum,Me}Zn(OH)** and sealed with a rubber septum. The reaction flask was attached to a Schlenk line, pump/purged 5 times, and finally left under nitrogen. Using a purged syringe, 2 mL distilled and degassed methanol was added, and the reaction stirred for 2 h under nitrogen. The reaction was then opened to air and stirred for 20 h upon which crude product precipitated from the reaction mixture. The product was collected by vacuum filtration and purified by column chromatography (basic alumina, 50% ethyl acetate in hexanes) to yield 91 mg (54%) of the biradical **5-T$_2$**. The product was crystallized from slow evaporation of a solution composed of a few drops of acetonitrile in *n*-pentane. IR (solid) ν_{max} (cm^{-1}): 2550 (w, BH). EPR (X-Band, 298 K): pentet (1:2:3:2:1), apparent a_N = 3.8 G. Mass spectrometry (m/z): 1157.4630 (M + H)$^+$.

■ ASSOCIATED CONTENT

Ⓢ Supporting Information

Synthesis and EPR spectra **SQ-T** (and regiospecifically deuterated **SQ-T** for hyperfine coupling constant assignment) as well as X-ray crystallographic details of biradical complexes. This information is available free of charge via the Internet at http://pubs.acs.org.

■ AUTHOR INFORMATION

Corresponding Authors

shultz@ncsu.edu
mkirk@unm.edu

Present Addresses

[§]Cree, Inc., Morrisville, NC.
[∥]Combi-Blocks, San Diego, CA.
[#]Advanced Liquid Logic, Morrisville, NC.
[⊥]Department of Chemistry, University of Western Ontario, London, Ontario, Canada.

Notes

The authors declare no competing financial interest.

■ ACKNOWLEDGMENTS

M.L.K. acknowledges the National Science Foundation (NSF CHE-1301142) for financial assistance. D.A.S. thanks the National Science Foundation (CHE-0910585/1213269) for financial support.

■ REFERENCES

(1) Wasielewski, M. R. *Chem. Rev.* **1992**, *92*, 435.
(2) Wenger, O. S. *Chem. Soc. Rev.* **2011**, *40*, 3538.
(3) Davis, W. B.; Svec, W. A.; Ratner, M. A.; Wasielewski, M. R. *Nature* **1998**, *396*, 60.
(4) Miller, S.; Lukas, A.; Marsh, E.; Bushard, P.; Wasielewski, M. *J. Am. Chem. Soc.* **2000**, *122*, 7802.
(5) Davis, W. B.; Ratner, M. A.; Wasielewski, M. R. *Chem. Phys.* **2002**, *281*, 333.
(6) Weiss, E. A.; Ratner, M. A.; Wasielewski, M. R. *J. Phys. Chem. A* **2003**, *107*, 3639.
(7) Weiss, E. A.; Ahrens, M. J.; Sinks, L. E.; Gusev, A. V.; Ratner, M. A.; Wasielewski, M. R. *J. Am. Chem. Soc.* **2004**, *126*, 5577.
(8) Sinks, L. E.; Weiss, E. A.; Giaimo, J. M.; Wasielewski, M. R. *Chem. Phys. Lett.* **2005**, *404*, 244.
(9) Weiss, E. A.; Tauber, M. J.; Kelley, R. F.; Ahrens, M. J.; Ratner, M. A.; Wasielewski, M. R. *J. Am. Chem. Soc.* **2005**, *127*, 11842.
(10) Weiss, E. A.; Wasielewski, M. R.; Ratner, M. A. *J. Chem. Phys.* **2005**, *123*, 064504.
(11) Goldsmith, R. H.; Wasielewski, M. R.; Ratner, M. A. *J. Phys. Chem. B* **2006**, *110*, 20258.
(12) Solomon, G. C.; Andrews, D. Q.; Hansen, T.; Goldsmith, R. H.; Wasielewski, M. R.; Van Duyne, R. P.; Ratner, M. A. *J. Chem. Phys.* **2008**, *129*, 054701.
(13) Ricks, A. B.; Solomon, G. C.; Colvin, M. T.; Scott, A. M.; Chen, K.; Ratner, M. A.; Wasielewski, M. R. *J. Am. Chem. Soc.* **2010**, *132*, 15427.
(14) Kirk, M. L.; Shultz, D. A. *Coord. Chem. Rev.* **2013**, *257*, 218.
(15) Hush, N. S. *Coord. Chem. Rev.* **1985**, *64*, 135.
(16) Barbara, P. F.; Meyer, T. J.; Ratner, M. A. *J. Phys. Chem.* **1996**, *100*, 13148.

(17) Tuczek, F.; Solomon, E. I. *Coord. Chem. Rev.* **2001**, *219*, 1075.
(18) Kirk, M. L.; Shultz, D. A.; Depperman, E. C.; Brannen, C. L. *J. Am. Chem. Soc.* **2007**, *129*, 1937.
(19) Blondin, G.; Girerd, J. J. *Chem. Rev.* **1990**, *90*, 1359.
(20) Kirk, M. L.; Shultz, D. A.; Depperman, E. C.; Habel-Rodriguez, D.; Schmidt, R. D. *J. Am. Chem. Soc.* **2012**, *134*, 7812.
(21) Kirk, M. L.; Shultz, D. A.; Habel-Rodriguez, D.; Schmidt, R. D.; Sullivan, U. *J. Phys. Chem. B* **2010**, *114*, 14712.
(22) Kirk, M. L.; Shultz, D. A.; Schmidt, R. D.; Habel-Rodriguez, D.; Lee, H.; Lee, J. *J. Am. Chem. Soc.* **2009**, *131*, 18304.
(23) Kirk, M. L.; Shultz, D. A.; Depperman, E. C. *Polyhedron* **2005**, *24*, 2880.
(24) Shultz, D. A.; Vostrikova, K. E.; Bodnar, S. H.; Koo, H.-J.; Whangbo, M.-H.; Kirk, M. L.; Depperman, E. C.; Kampf, J. W. *J. Am. Chem. Soc.* **2003**, *125*, 1607.
(25) Kondo, M.; Tada, T.; Yoshizawa, K. *J. Phys. Chem. A* **2004**, *108*, 9143.
(26) Maya, F.; Tour, J. M. *Tetrahedron* **2004**, *60*, 81.
(27) Silva, C. A. B.; da Silva, S. J. S.; Leal, J. F. P.; Pinheiro, F. A.; Del Nero, J. *Phys. Rev. B* **2011**, 83.
(28) Nishizawa, S.; Hasegawa, J.; Matsuda, K. *Chem. Phys. Lett.* **2013**, *555*, 187.
(29) Wasielewski, M. R.; Miura, T. *J. Am. Chem. Soc.* **2011**, *133*, 2844.
(30) Shi, S. W.; Jiang, P.; Chen, S.; Sun, Y. P.; Wang, X. C.; Wang, K.; Shen, S. L.; Li, X. Y.; Li, Y. F.; Wang, H. Q. *Macromolecules* **2012**, *45*, 7806.
(31) Luo, Y.; Wang, C. K.; Fu, Y. *Chem. Phys. Lett.* **2003**, *369*, 299.
(32) James, D. K.; Tour, J. M. In *Molecular Wires: From Design to Properties*; DeCola, L., Ed.; Springer: Berlin, **2005**; Vol. *257*, p 33.
(33) Xu, B. Q. Q.; Li, X. L. L.; Xiao, X. Y. Y.; Sakaguchi, H.; Tao, N. J. J. *Nano Lett.* **2005**, *5*, 1491.
(34) Whalley, A. C.; Steigerwald, M. L.; Guo, X.; Nuckolls, C. *J. Am. Chem. Soc.* **2007**, *129*, 12590.
(35) Peng, G.; Strange, M.; Thygesen, K. S.; Mavrikakis, M. *J. Phys. Chem. C* **2009**, *113*, 20967.
(36) Smaali, K.; Lenfant, S.; Karpe, S.; Ocafrain, M.; Blanchard, P.; Deresmes, D.; Godey, S.; Rochefort, A.; Roncali, J.; Vuillaume, D. *ACS Nano* **2010**, *4*, 2411.
(37) Park, B.; Aiyar, A.; Park, M. S.; Srinivasarao, M.; Reichmanis, E. *J. Phys. Chem. C* **2011**, *115*, 11719.
(38) Shoute, L. C. T.; Pekas, N.; Wu, Y. L.; McCreery, R. L. *Appl. Phys. A: Mater. Sci. Process.* **2011**, *102*, 841.
(39) Kumar, R.; Pillai, R. G.; Pekas, N.; Wu, Y. L.; McCreery, R. L. *J. Am. Chem. Soc.* **2012**, *134*, 14869.
(40) Fan, J. P.; Gathitu, N. N.; Chang, Y. F.; Zhang, J. P. *J. Chem. Phys.* **2013**, *138*, 074307.
(41) Lamba, V. K.; Engles, S. J.; Sawhney, R. S.; Arora, C.; Engles, D. *Mol. Phys.* **2013**, *111*, 517.
(42) Shokri, R.; Lacour, M. A.; Jarrosson, T.; Lere-Porte, J. P.; Serein-Spirau, F.; Miqueu, K.; Sotiropoulos, J. M.; Vonau, F.; Aubel, D.; Cranney, M.; Reiter, G.; Simon, L. *J. Am. Chem. Soc.* **2013**, *135*, 5693.
(43) Yan, H. J.; Bergren, A. J.; McCreery, R.; Della Rocca, M. L.; Martin, P.; Lafarge, P.; Lacroix, J. C. *Proc. Natl. Acad. Sci. U.S.A.* **2013**, *110*, 5326.
(44) Lambert, C.; Nöll, G. *J. Am. Chem. Soc.* **1999**, *121*, 8434.
(45) Rosokha, S. V.; Sun, D.-L.; Kochi, J. K. *J. Phys. Chem. A* **2002**, *106*, 2283.
(46) Reuter, L. G.; Bonn, A. G.; Stuckl, A. C.; He, B. C.; Pati, P. B.; Zade, S. S.; Wenger, O. S. *J. Phys. Chem. A* **2012**, *116*, 7345.
(47) Eng, M. P.; Albinsson, B. *Chem. Phys.* **2009**, *357*, 132.
(48) Wenger, O. S.; Hankache, J. *Chem. Rev.* **2011**, *111*, 5138.
(49) Liu, C.-Y.; Gavryushin, A.; Knochel, P. *Chem. Asian J.* **2007**, *2*, 1020.
(50) Shultz, D. A.; Hollomon, M. G. *Chem. Mater.* **2000**, *12*, 580.
(51) Shimono, S.; Tamura, R.; Ikuma, N.; Takimoto, T.; Kawame, N.; Tamada, O.; Sakai, N.; Matsuura, H.; Yamauchi, J. *J. Org. Chem.* **2004**, *69*, 475.
(52) Ruf, M.; Vahrenkamp, H. *Inorg. Chem.* **1996**, *35*, 6571.
(53) Ruf, M.; Noll, B. C.; Groner, M. D.; Yee, G. T.; Pierpont, C. G. *Inorg. Chem.* **1997**, *36*, 4860.
(54) Shultz, D. A.; Bodnar, S. H.; Vostrikova, K. E.; Kampf, J. W. *Inorg. Chem.* **2000**, *39*, 6091.
(55) Weiser, P. T.; Williams, A. B.; Chang, C.-Y.; McDonnell, D. P.; Hanson, R. N. *Bioorg. Med. Chem. Lett.* **2012**, *22*, 6587.
(56) Magdziak, D.; Rodriguez, A. A.; Van De Water, R. W.; Pettus, T. R. R. *Org. Lett.* **2002**, *4*, 285.
(57) Chu, H.-C.; Sahu, D.; Hsu, Y.-C.; Patra, D.; Lin, J.-T.; Bhattacharya, D.; Lu, K.-L.; Wei, K.-H.; Lin, H.-C. *Dyes Pigm.* **2012**, *93*, 1488.
(58) Kirk, M. L.; Shultz, D. A.; Stasiw, D. E.; Habel-Rodriguez, D.; Stein, B.; Boyle, P. D. *J. Am. Chem. Soc.* **2013**, *135*, 14713.
(59) Kirk, M. L.; Shultz, D. A.; Stasiw, D. E.; Lewis, G. F.; Wang, G.; Brannen, C. L.; Sommer, R. D.; Boyle, P. D. *J. Am. Chem. Soc.* **2013**, 135.
(60) Lanfranc de Panthou, F.; Luneau, K.; Musin, R.; Öhrström, L.; Grand, A.; Turek, P.; Rey, P. *Inorg. Chem.* **1996**, *35*, 3484.
(61) de Panthou, F. L.; Luneau, D.; Laugier, J.; Rey, P. *J. Am. Chem. Soc.* **1993**, *115*, 9095.
(62) de Panthou, F. L.; Luneau, D.; Musin, R.; Öhrström, L.; Grand, A.; Turek, P.; Rey, P. *Inorg. Chem.* **1996**, *35*, 3484.
(63) See Supporting Information.
(64) Herring, C.; Flicker, M. *Phys. Rev.* **1964**, *134*, A362.
(65) de Kanter, F. J. J.; Sagdeev, R. Z.; Kaptein, R. *Chem. Phys. Lett.* **1978**, *58*, 334.
(66) Weller, A.; Staerk, H.; Treichel, R. *Faraday Discuss. Chem. Soc.* **1984**, *78*, 271.
(67) McConnell, H. M.; McLachlan, A. D. *J. Chem. Phys.* **1961**, *34*, 1.
(68) Wold, D. J.; Haag, R.; Rampi, M. A.; Frisbie, C. D. *J. Phys. Chem. B* **2002**, *106*, 2813.
(69) Helms, A.; Heiler, D.; McLendon, G. *J. Am. Chem. Soc.* **1992**, *114*, 6227.
(70) Yamada, R.; Kumazawa, H.; Noutoshi, T.; Tanaka, S.; Tada, H. *Nano Lett.* **2008**, *8*, 1237.
(71) Ikemoto, J.; Takimiya, K.; Aso, Y.; Otsubo, T.; Fujitsuka, M.; Ito, O. *Org. Lett.* **2002**, *4*, 309.
(72) Nakamura, T.; Fujitsuka, M.; Araki, Y.; Ito, O.; Ikemoto, J.; Takimiya, K.; Aso, Y.; Otsubo, T. *J. Phys. Chem. B* **2004**, *108*, 10700.
(73) Beek, W. J. E.; Janssen, R. A. J. *J. Mater. Chem.* **2004**, *14*, 2795.
(74) Eng, M. P.; Albinsson, B. *Angew. Chem., Int. Ed.* **2006**, *45*, 5626.
(75) Evenson, J. W.; Karplus, M. *J. Chem. Phys.* **1992**, *96*, 5272.
(76) Evenson, J. W.; Karplus, M. *Science* **1993**, *262*, 1247.
(77) Goldsmith, R. H.; Sinks, L. E.; Kelley, R. F.; Betzen, L. J.; Liu, W. H.; Weiss, E. A.; Ratner, M. A.; Wasielewski, M. R. *Proc. Natl. Acad. Sci. U.S.A.* **2005**, *102*, 3540.
(78) McConnell, H. M. *J. Chem. Phys.* **1961**, *35*, 508.
(79) Gray, H. B.; Winkler, J. R. *Proc. Natl. Acad. Sci. U.S.A.* **2005**, *102*, 3534.
(80) Wenger, O. S. *Acc. Chem. Res.* **2011**, *44*, 25.